Wounded quarks in $A + A$, $p + A$, and $p + p$ collisions

Piotr Bożek,[1,*] Wojciech Broniowski,[2,3,†] and Maciej Rybczyński[3,‡]

[1]*AGH University of Science and Technology, Faculty of Physics and Applied Computer Science, al. Adama Mickiewicza 30, 30-059 Cracow, Poland*

[2]*The Henryk Niewodniczański Institute of Nuclear Physics, Polish Academy of Sciences, 31-342 Cracow, Poland*

[3]*Institute of Physics, Jan Kochanowski University, 25-406 Kielce, Poland*

(Received 3 May 2016; revised manuscript received 6 June 2016; published 5 July 2016)

We explore predictions of the wounded-quark model for particle production and properties of the initial state formed in ultrarelativistic heavy-ion collisions. The approach is applied uniformly to $A + A$ collisions in a wide collision energy range, as well as for $p + A$ and $p + p$ collisions at the CERN Large Hadron Collider (LHC). We find that generically the predictions from wounded quarks for such features as eccentricities or initial sizes are close (within 15%) to predictions of the wounded nucleon model with an amended binary component. A larger difference is found for the size in $p + \mathrm{Pb}$ system, where the wounded-quark model yields a smaller (more compact) initial fireball than the standard wounded-nucleon model. The inclusion of subnucleonic degrees of freedom allows us to analyze $p + p$ collisions in an analogous way, with predictions that can be used in further collective evolution. The approximate linear dependence of particle production in $A + A$ collisions on the number of wounded quarks, as found in previous studies, makes the approach based on wounded quarks natural. Importantly, at the LHC energies we find approximate uniformity in particle production from wounded quarks, where at a given collision energy per nucleon pair similar production of initial entropy per source is needed to explain the particle production from $p + p$ collisions up to $A + A$ collisions. We also discuss the sensitivity of the wounded-quark model predictions to distribution of quarks in nucleons, distribution of nucleons in nuclei, and the quark-quark inelasticity profile in the impact parameter. In our procedure, the quark-quark inelasticity profile is chosen in such a way that the experiment-based parametrization of the proton-proton inelasticity profile is properly reproduced. The parameters of the overlaid multiplicity distribution are fixed from $p + p$ and $p + \mathrm{Pb}$ data.

DOI: 10.1103/PhysRevC.94.014902

I. INTRODUCTION

The idea of wounded quarks [1,2] was proposed shortly after the successful concept of wounded nucleons [3], in the quest of understanding in a natural way particle production in high-energy nuclear collisions. In particular, in these early applications one looked for appropriate scaling of particle production with the number of participants, and the idea of *wounding*, i.e., production from a participant independent on the number of its collision with participants from the other nucleus, proved very useful. It is based on the Glauber approach [4] adapted to inelastic collisions [5], and the soft particle production may be justified in terms of the Landau-Pomeranchuk effect (for review, see Ref. [6]).

With the advent of the BNL Relativistic Heavy-Ion Collider (RHIC), the idea of wounded nucleons was revived by the PHOBOS Collaboration [7]. However, to explain the multiplicity distribution in $\mathrm{Au} + \mathrm{Au}$ collisions, it was necessary to include a component proportional to the binary collisions [8], i.e., depending nonlinearly on the number of the wounded nucleons. Then the average number of particles produced at midrapidity is

$$\frac{dN_{\mathrm{ch}}}{d\eta} \sim \frac{1-\alpha}{2} N_{\mathrm{W}} + \alpha N_{\mathrm{bin}}, \tag{1}$$

where N_{W} denotes the number of wounded nucleons and N_{bin} the number of binary collisions, with the first term interpreted as soft production and the second as hard production [8].

In heavy-ion phenomenology, the entropy density profile in the initial state is the most important source of uncertainty in hydrodynamic models. Besides the Monte Carlo Glauber initial condition, IP (impact-parameter-dependent) glasma and Kharzeev-Levin-Nardi initial conditions are frequently used [9,10]. One should note that differences in the parametrizations of the initial entropy deposition give different eccentricities of the fireball [11]. Within the Monte Carlo Glauber approach, an understanding in more microscopic terms of the phenomenological binary collisions component in Eq. (1) is desired, whereby uncertainties in the initial entropy deposition in the Glauber model should be reduced.

Eremin and Voloshin [12] noticed that the RHIC multiplicity data can be naturally reproduced within a wounded-quark model. With a larger number of constituents (three with quarks) and a reduced cross section of quarks compared to nucleons, one can obtain an approximately linear increase in particle production with the number of wounded quarks, denoted as Q_{W} in this paper, namely,

$$\frac{dN_{\mathrm{ch}}}{d\eta} \sim Q_{\mathrm{W}}. \tag{2}$$

*Piotr.Bozek@fis.agh.edu.pl
†Wojciech.Broniowski@ifj.edu.pl
‡Maciej.Rybczynski@ujk.edu.pl

The quark scaling has also been reported for the SPS energies [13]. It has been vigorously promoted by the PHENIX Collaboration [14,15]. Experimental data on particle production have been compared to the number of wounded nucleons or wounded quarks. The number of wounded quarks or nucleons in a collisions is obtained from a Glauber Monte Carlo code [16,17], where for the model with quark constituents additionally three quarks are distributed in each nucleon and collisions occur between pairs of quarks. An approximate, uniform scaling of the multiplicity and of the transverse energy with the number of wounded quarks is claimed [14,15], also including the LHC data [18]. The elliptic flow fluctuation measurements were compared to the wounded-nucleon and wounded-quark models by the STAR Collaboration in Ref. [19].

The basic effect of the subnucleonic degrees of freedom in particle production is a stronger combinatorics, which accomplishes the approximately linear scaling of production with the number of constituents. An intermediate combinatorics is realized in the quark-diquark model [20], which led to proper description of the RHIC data as well as the proton-proton scattering amplitude (including the differential elastic cross section) at energies available at the CERN Intersecting Storage Rings (ISR).

The purpose of this paper is to explore in detail predictions of the wounded-quark approach to particle production and properties of the initial state, as well as to investigate sensitivity to the assumptions concerning the distribution of quarks and the quark-quark collision profile. While this work was nearing completion, a similar study for $A + A$ collisions by Zheng and Yin [21] appeared. In Ref. [18] the scaling of particle production with the number of quarks is discussed, whereas in Ref. [22] different ways of generating quark positions in the nucleon are compared. In addition, Loizides [23] presented a detailed study of the initial state in heavy-ion collisions for models involving a number of partons in a nucleon different than three.

The difference in this work compared to other studies is that our methodology fixes the proton shape and the quark-quark inelasticity profile to reproduce accurately the inelasticity profile in proton-proton collisions. It is important, because the details of the model of partons in nuclei, such as the effective size of the nucleon, the quark-quark cross section, and the shape of the inelasticity profile in quark-quark scattering turn out to be important for the results. With the fitted parameters of the quark distribution in nucleons and quark scattering, we calculate the basic characteristics (eccentricities, sizes, and their event-by-event fluctuations) of the initial state in $A + A$ collisions. We also apply the approach to $p + A$ and $p + p$ collisions, not analyzed in other works. This extension is important, as it checks consistency of the constituent quark scaling, as well as probes the limit of collectivity in small systems.

The outline of our paper is as follows. In Sec. II A we present our method of fixing the parameters of the model in terms of the proton-proton scattering amplitude, with further details given in the Appendix. Next, we discuss the overlaying of fluctuations on the Glauber sources, with the Γ distribution in the initial stage and the Poisson distribution at hadronization, convolving to the popularly used negative binomial distribution. These extra fluctuations are necessary to describe the $p + A$ and $p + p$ collisions or the $A + A$ collisions at lowest centralities; they also contribute to eccentricities or event-by-event fluctuation measures. In Sec. III we look at the $A + A$ collisions at a wide energy range, testing the wounded-quark scaling of hadron production and its sensitivity to model assumptions. We then pass to the study of eccentricities (including the hypercentral U + U collisions) and size fluctuations. Section IV presents the results for $p + A$ collisions, where we use the measured multiplicity distributions of produced hadrons to fix the parameters of the overlaid distribution. We then obtain the eccentricities and sizes of the initial fireball. We find that in the case of wounded quarks the initial size is significantly more compact than in the standard wounded-nucleon model. In Sec. V we analyze in an analogous way the $p + p$ collisions, which is possible with subnucleonic degrees of freedom. The obtained initial fireballs for highest-multiplicity $p + p$ collisions could be used in studies of subsequent collective evolution of the system. The possibility of including more wounded constituents is explored in Sec. VI. Finally, Sec. VII contains our summary, with the main conclusion that the concept of wounded quarks works uniformly from $p + p$ to Pb + Pb collisions at the LHC energies, providing approximately linear scaling of hadron production with the number of sources, and resulting in properties of the initial fireball close to the predictions with wounded nucleons amended with binary collisions. At RHIC we observe dependence of the scaling on the colliding nuclei and substantial difference with the $p + p$ channel (about 30%), which indicates the need for improvement of the theoretical description at lower collision energies.

II. GENERAL FORMULATION

A. Quarks inside nucleons

Constituent quarks are localized within nucleons, which results in their clustering as opposed to free, unconfined distribution in the nucleus. For that reason we attempt to model their distributions in a realistic way. First, we randomly place the centers of quarks in the nucleons according to the radial distribution

$$\rho(r) = \frac{r^2}{r_0^3} e^{-r/r_0}, \tag{3}$$

with a shift to the center of mass of the nucleon after generating the positions of the three quarks. Positions of nucleons in a nucleus are distributed according to a standard Woods-Saxon radial density profile with appropriate parameters [24,25] or are taken from outside microscopic calculations, such as Ref. [26]. Nuclear deformation [27–30] is incorporated for deformed nuclei, such as ^{63}Cu, ^{197}Au, or ^{238}U, used at RHIC.

The quark-quark wounding profile (inelasticity profile in the impact parameter b) is for simplicity assumed to have the Gaussian shape

$$p_{\rm qq}^{\rm in}(b) = 2\pi b e^{-\pi b^2/\sigma_{\rm qq}}, \tag{4}$$

where $\sigma_{\rm qq}$ is the quark-quark inelastic cross section.

The choice of this profile, together with the parametrization (3), is important, as it determines the probability of a collision at the transverse separation b, which influences the wounded-quark scaling and the properties of the formed initial state. The numbers r_0 and σ_{qq} are treated as adjustable parameters and, at each collision energy, are fitted to the nucleon-nucleon total inelastic cross section and to the nucleon-nucleon inelasticity profile. The latter can be obtained straightforwardly from working parametrizations of the NN scattering data, which describe both inelastic and elastic collision amplitudes. Here we take the parametrization of Ref. [31] based on the Barger-Phillips model [32]. The details of our procedure are given in the Appendix. The bottom line of this procedure is that we reproduce with sufficient accuracy the experimental inelasticity profile of the NN collisions. The values of our parameters are listed in Table I in the Appendix.

In the wounded-quark Glauber model of the PHENIX Collaboration [14,15], the size of the proton is energy independent, whereas the quark-quark cross section increases with the collision energy. In a different approach, the increase of the nucleon-nucleon cross section with energy is achieved with the increase of the nucleon size [33]. When fitting the inelastic profile at different energies in our approach we find that the effective size of the nucleon increases very weakly with the energy, while the quark-quark cross section increases sizably with the energy. The corresponding change in the quark-quark inelasticity profile is determined by σ_{qq}; cf. Eq. (4).

B. Overlaid distribution

The number of particles produced in $p + p$ collisions fluctuates. In the wounded-quark model only a part of these fluctuations can be accounted for by fluctuations of the number of wounded quarks in a collision. To describe the experimentally measured distributions, the charged hadron distribution should be written as a convolution of the numbers of hadrons n_k produced from each wounded quark,

$$P(n) = \sum_i P_{\rm wq}(i) \times \sum_{n_1,n_2,\ldots,n_i} P_{\rm hq}(n_1)P_{\rm hq}(n_2)\cdots P_{\rm hq}(n_i)\delta_{n,n_1+n_2+\cdots+n_i}, \tag{5}$$

where $P_{\rm wq}$ is the distribution of the number i of wounded quarks and $P_{\rm hq}$ is the overlaid distribution of the number of hadrons from an individual wounded quark. The above formula should be used uniformly for $p + p$, $p + A$, and $A + A$ collisions if the production mechanism is to be universal. In the following we use the negative binomial distribution to parametrize $P_{\rm hq}$, namely,

$$P_{\rm NB}(n|\bar{n},\kappa) = \frac{\Gamma(n+\kappa)\bar{n}^n\kappa^\kappa}{\Gamma(\kappa)n!(\bar{n}+\kappa)^{n+\kappa}}, \tag{6}$$

where $\Gamma(z)$ is the Euler Γ function, the average is given by $\bar{n}$, and $\kappa = \bar{n}^2/[{\rm var}(n) - \bar{n}]$ (larger κ means smaller fluctuations). This form has been widely used to describe the multiplicity distributions in $p + p$ collisions [34]. The parameters $\bar{n}$ and κ of the negative binomial distribution can be adjusted to reproduce the observed multiplicity distribution in $p + p$ (Sec. V) or $p + A$ collisions (Sec. IV A). In collisions of heavy nuclei the multiplicity distribution, or the mean multiplicity in each centrality bin, is almost independent on the overlaid distribution, except for very central collisions, where it should be taken into account. However, effects of the overlaid distribution show up also in $A + A$ collisions in various event-by-event fluctuation quantities.

When dividing the dynamics of the collision into two stages, namely (1) the formation of the initial fireball and (2) its subsequent evolution and decay into hadrons, one should also separate the multiplicity fluctuations into two corresponding parts. The first part comes from the fluctuations in the initial entropy deposition in the fireball, whereas the other part comes from entropy production during the expansion of the fireball and subsequent hadronization. Note that a smooth, linear increase of entropy in viscous hydrodynamics is effectively included in the normalization coefficient. We neglect possible fluctuations in the hydrodynamic phase [35,36] (which are expected not to be very large [37]) and from correlated particle emissions at freeze-out. We follow the usual assumption that the particle emission is given by a Poisson process, with the mean proportional to the entropy in the fluid element.

As the negative binomial distribution is a convolution of the Γ and the Poisson distributions, the entropy distribution $P(s)$ in the fireball is given by a convolution of a Γ distribution,

$$P_\Gamma(s|\bar{n},\kappa) = \frac{s^{\kappa-1}\kappa^\kappa}{\Gamma(\kappa)\bar{n}^\kappa}e^{-\kappa s/\bar{n}}, \tag{7}$$

with the distribution of the number of wounded quarks,

$$P(s) = \sum_i P_{\rm wq}(i)P_\Gamma(s|i\bar{n},i\kappa). \tag{8}$$

Microscopically, it means that each wounded quark deposits a random entropy s taken from the Γ distribution (7), with same parameters as the parameters of the negative binomial distribution adjusted to the multiplicity distributions. The fluctuations in entropy deposition increase the fluctuations and deformations of the initial fireball. The effect is especially important in small systems or for central $A + A$ collisions [30,38–40]. Throughout this work, according to the above discussion, we overlay a negative binomial distribution on top of the wounded-quark distribution when calculating the hadron multiplicity distribution in $p + p$ and $p + A$ collisions, and we overlay a Γ distribution when calculating the entropy profile of the initial fireball and its properties, such as eccentricities or size.

C. Smearing of sources

On physical grounds, the Glauber sources must possess a certain transverse size; smoothness of the initial condition is also required by hydrodynamics. For that reason one needs to smooth the initial distribution. We follow the Gaussian prescription, where the entropy density from a single source centered at a transverse point (x_0, y_0) is given with the profile

$$g(x,y) = \frac{1}{2\pi\sigma^2}\exp\left[-\frac{(x-x_0)^2+(y-y_0)^2}{2\sigma^2}\right]. \tag{9}$$

Unless otherwise stated, we use arbitrarily $\sigma = 0.2$ fm in the wounded-quark model and $\sigma = 0.4$ fm in the wounded-nucleon model. One should note that in small systems the fireball eccentricities or sizes depend sensitively on the value of σ.

D. Methodology

Our modeling concerns the initial stage of the collision. To describe physical observables in a complete way, modeling of later stages is necessary, such as hydrodynamics or transport in the intermediate stage, followed with hadronization. To avoid these complications, in this paper, following a common practice, we select observables which are not sensitive to the details of the intermediate evolution. Thus, for multiplicities the basic assumption is that the production of physical hadrons is proportional to the initially deposited entropy [41–43]. It is supported with simulations in ideal and viscous hydrodynamics [44–46]. For the flow, the linear response of the system to small perturbation (see, e.g., Ref. [47–49]) leads to approximate relations linking the elliptic and triangular flow coefficients to eccentricities (the shape-flow transmutation). Namely, $v_n \simeq \kappa_n \varepsilon_n$, $n = 2,3$, where κ_n depends on the collision energy, centrality, or rank n, but not on ε_n itself. This feature allows us to obtain results for the ratios of moments of v_n, which are approximately equal to the corresponding ratios of moments of ε_n. A similar argumentation is used to link the initial size fluctuations to the measurable transverse momentum fluctuations [50].

III. $A + A$ COLLISIONS

A. Multiplicity distribution

We begin the presentation of our results by showing the outcome of the wounded-quark model for the $A + A$ collisions. The results, obviously, depend on the centrality of the collision, which is defined experimentally via the response of detectors; hence, its detailed modeling may be complicated. Assuming that the centrality is obtained from the multiplicity of the collision, we may evaluate it as percentiles of the event-by-event distribution of the number of sources, which is accurate enough except for the very central and very peripheral events [51]. A better way is to obtain centrality from the number of sources with weights from an overlaid distribution (see Sec. II B). However, in presenting the results in the field it is customary to use the number of wounded *nucleons* $N_{\rm W}$, as obtained from the Glauber simulations with the model of Eq. (1). We follow this convention; thus, $N_{\rm W}$ serves as a label for the centrality classes, even when these are determined by the wounded quarks.

The basic test of the wounded-quark model is its very definition of Eq. (2), whereby the production of hadrons should be proportional to the number of wounded quarks $Q_{\rm W}$. In particular, the ratio of the multiplicity of charged hadrons at midrapidity $dN_{\rm ch}/d\eta$ divided by $Q_{\rm W}$, should not depend on centrality or on colliding nuclei. To find $Q_{\rm W}$ corresponding to a given centrality we have carried out simulations in the Glauber model with the help of an appropriately modified GLISSANDO code [24,38]. In the standard calculation, the nuclear profiles of heavy nuclei are obtained from the Woods-Saxon form

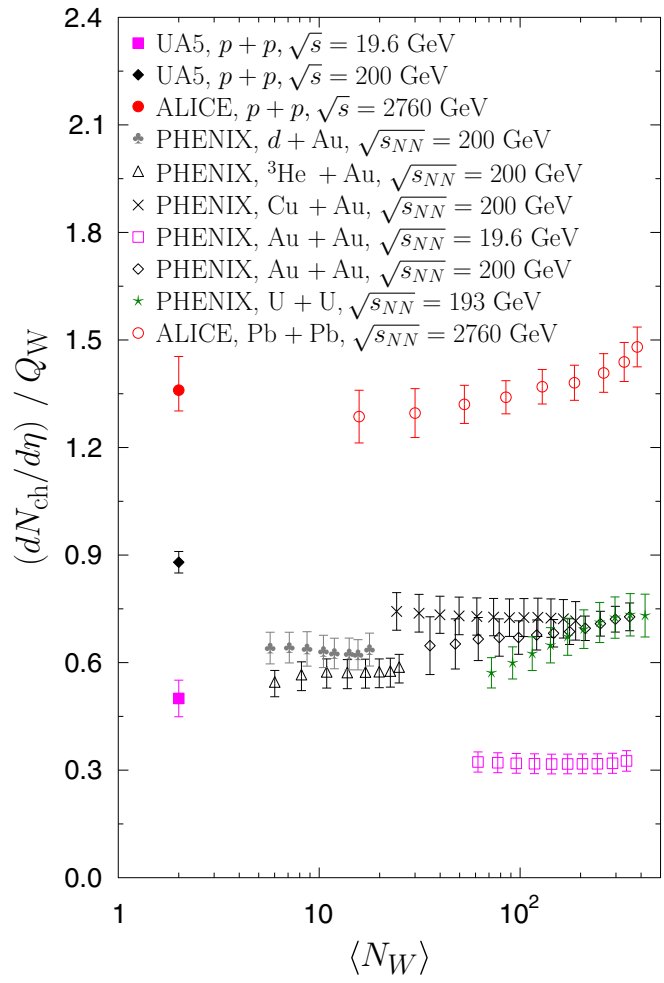

FIG. 1. Experimental multiplicity of charged hadrons per unit of pseudorapidity (at midrapidity) divided by the number of wounded quarks, $dN_{\rm ch}/d\eta/Q_{\rm W}$, plotted as a function of centrality expressed via the number of wounded nucleons. We also show the results for the $p + p$ collisions (solid symbols at $\langle N_{\rm W}\rangle = 2$) discussed in Sec. V. The data are from Refs. [15,54–56].

with the nucleon-nucleon expulsion radius of 0.9 fm [52]. For the deuteron we use the Hulthen wave function, and for ^{3}He we take the distributions from the method of Ref. [53] as provided in Ref. [17]. The quarks are then generated in nucleons according to Eq. (3), whereas the inelasticity profile for the quark-quark collisions is of the Gaussian form (4).

The results are shown in Fig. 1. We note that, in qualitative agreement with the earlier studies [12–15], the dependence of $dN_{\rm ch}/d\eta/Q_{\rm W}$ on centrality is approximately flat and increases with the collision energy. We note that some deviation from a linear scaling between the initial entropy and the final particle density in pseudorapidity is possible owing to different mean transverse momentum or different entropy production at different centralities [44] during the evolution of the system. In contrast, the flatness is not the case of the wounded-nucleon model of Eq. (1), where, as is well known, the ratio $dN_{\rm ch}/d\eta/N_{\rm W}$ increases considerably with $N_{\rm w}$. Moreover, the

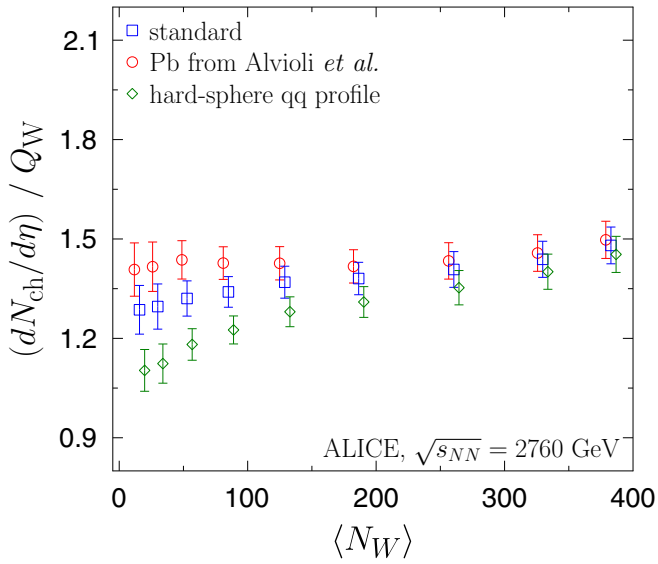

FIG. 2. Comparison of $dN_{\rm ch}/d\eta/Q_{\rm W}$ in Pb + Pb collisions at $\sqrt{s_{NN}} = 2.76$ TeV [56], obtained with the standard GLISSANDO simulations with the nuclear Woods-Saxon distribution (squares), compared to the case of correlated nuclear distributions of Alvioli *et al.* from Ref. [26]. We also show the calculation with quarks implemented as in the Glauber Monte Carlo of Refs. [15,23] (diamonds), i.e., with the nucleon profile from Ref. [15] and a hard-sphere quark-quark inelasticity profile.

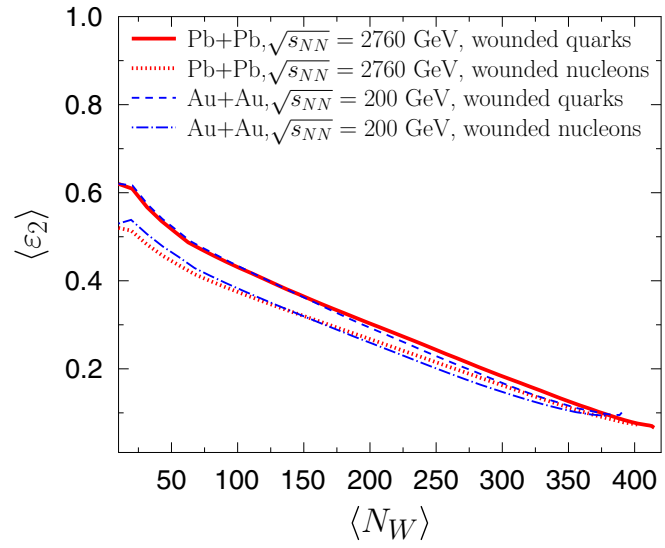

FIG. 3. Average ellipticity vs centrality for two selected reactions, evaluated in the wounded-quark and wounded-nucleon models.

value of $dN_{\rm ch}/d\eta/Q_{\rm W}$ (i.e., the average number of charge hadrons per unit of rapidity coming from a single wounded quark), is, at a given energy, roughly similar for various considered reactions. For the LHC energies it is also consistent with the $p + p$ collisions, where the data are taken from Ref. [55] and $Q_{\rm W}$ is obtained in Sec. V. At RHIC energies of $\sqrt{s_{NN}} =$ 200 and 19.6 GeV the $p + p$ point, obtained with the data from Ref. [54], is noticeably higher (about 30%) than the band for the $A + A$ collisions. Also, the dependence on the colliding nuclei at RHIC indicates a systematic uncertainly of the approach.

The above-discussed universality of the hadron production in $p + p$ vs $A + A$, holding fairly well for the LHC and to a lesser degree for the lower energies, is an important check of the idea of the independent production from the wounded-quark sources. We note that at lower energies it is not very accurate. Also, as the plots in Fig. 1 are not really flat, the wounded-quark scaling is approximate. This observation may suggest that the effective number of subnucleonic degrees of freedom at RHIC energies is smaller than three, as implied, e.g., by the quark-diquark model [20], and at higher energies may be larger than three (cf. Sec. VI).

To assess the sensitivity of the approximate wounded quark scaling for the particle production, we check the dependence on the nucleon distributions in nuclei, as well as on the treatment of quarks. First, in Fig. 2 we compare our standard GLISSANDO calculation described in Sec. II A with Woods-Saxon distributions (squares) to an analogous simulation with distributions obtained from Ref. [26], where central two-body nucleon-nucleon correlations are incorporated (circles). We note that the latter case yields an even more flat result as a function of centrality. The reason for this behavior is a longer tail in the one-body nucleon distributions of Ref. [26] as compared to the Woods-Saxon profile [24].

Second, we compare our standard results to the calculation made as in the quark Glauber Monte Carlo code described in Refs. [15,23] (diamonds), i.e., with a modified distribution of quarks in the nucleon and a hard-sphere quark-quark inelasticity profile (the resulting nucleon-nucleon inelasticity profile in this case is different from the experimental parametrization used in this paper; cf. the Appendix). We notice a substantial difference from our standard result, with a larger breaking of the wounded-quark scaling. The conclusion emerging from Fig. 2 is that the modeling of the subnucleonic structure should be done as accurately and realistically as possible. The same concerns the nuclear distributions, the distributions of quarks inside nucleons, or the quark-quark inelasticity profiles, as such details influence the bulk properties in $A + A$ collisions. Still some systematic errors, stemming from the model assumptions on the nuclear and subnucleonic structure of the nuclei, are unavoidable.

B. Eccentricities

A basic feature of phenomenology of relativistic heavy-ion collisions is the development of harmonic flow owing to geometry [58] and to event-by-event fluctuations [59–64]. In this section we compare predictions of the wounded-nucleon and wounded-quark models for the eccentricities of the initial state. For the wounded-nucleon case we use the mixing parameter $\alpha = 0.145$ for $\sqrt{s_{NN}} = 200$ GeV and $\alpha = 0.15$ for $\sqrt{s_{NN}} = 2.76$ TeV. The Gaussian smearing parameter is $\sigma = 0.4$ fm for wounded nucleons and $\sigma = 0.2$ fm for wounded quarks (the value of σ has tiny effects in the $A + A$ collisions). We note from Fig. 3 that the wounded quarks lead to larger ellipticity compared to the wounded-nucleon case, with the effect reaching about 15% at the peripheral collisions.

We have checked that for the most central collisions the ratio $\varepsilon_3/\varepsilon_2$ approaches the limit of the independent source

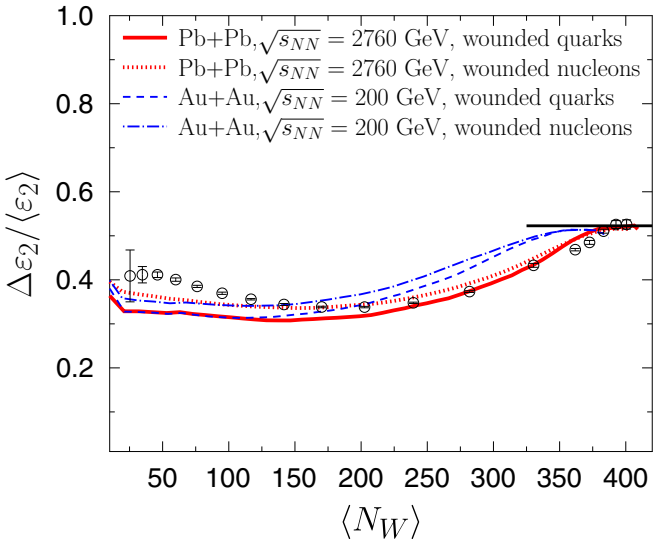

FIG. 4. The fluctuation measure $\Delta\varepsilon_2/\langle\varepsilon_2\rangle$ vs centrality, evaluated in the wounded-quark and wounded-nucleon models and compared to the data from ATLAS Collaboration [57] (circles).

model (cf. Eq. (7.8) of Ref. [65], see also the discussion in Ref. [66]), namely,

$$\frac{\varepsilon_3}{\varepsilon_2} = \frac{\langle\rho^2\rangle}{\langle\rho^3\rangle}\sqrt{\frac{\langle\rho^6\rangle}{\langle\rho^4\rangle}}, \tag{10}$$

where $\langle\rho^n\rangle$ denote the moments of the initial density for collisions at at zero impact parameter in the transverse radius $\rho = \sqrt{x^2+y^2}$. Numerically, the ratio of Eq. (10) is very similar for the wounded-nucleon and wounded-quark models and is ∼1.1. As is known, the proximity of the most central values of ε_2 and ε_3 leads to problems in the description of v_2 and v_3 in viscous hydrodynamics, where triangular flow is quenched more strongly than the elliptic flow [67]. As a result, the predicted values of v_3 are significantly smaller than v_2, in contrast to the experiment [68].

When switching from nucleon to quark participants two effects influence the entropy distribution in the fireball, with the opposite effect on the eccentricities. First, additional fluctuations at subnucleonic scales appear from individual entropy deposition from wounded quarks. Second, the entropy is spread around the nucleon-nucleon collision point among the different positions of individual wounded quarks in the colliding nucleons. The second effect can be estimated from the rms size of the fireball in $p+p$ collisions (Sec. V); it is of the same order (0.4 fm) as the width of the Gaussian centered at the positions of the wounded nucleons. The second effect comes in a similar way in both models and gives a reduction of the eccentricities. However, the first effect appears only when using subnucleonic degrees of freedom and leads to larger eccentricities in the wounded-quark model. Correspondingly, as presented in Fig. 4, scaled event-by-event fluctuations of ellipticity are reduced with wounded quarks, which brings the results closer to the data in semicentral collisions. The horizontal line in Fig. 4 corresponds to the limit of $\sqrt{4/\pi - 1}$ reached in the most central events [65].

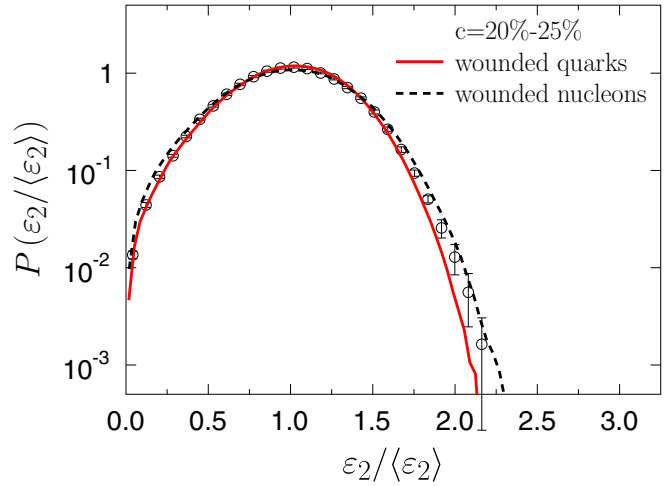

FIG. 5. Distribution of $\varepsilon_2/\langle\varepsilon_2\rangle$ for centrality 20%–25%, compared to the data for $v_2/\langle v_2\rangle$ from ATLAS Collaboration [57] (circles).

Results analogous to Figs. 3 and 4 for the triangularity are very similar for the wounded-quark and the wounded-nucleon models, except for $\langle\varepsilon_3\rangle$ at peripheral collisions, where wounded quarks give higher values than wounded nucleons, up to about 15%.

In Figs. 5 and 6 we compare the distributions of $\varepsilon_n/\langle\varepsilon_n\rangle$ for ellipticity ($n=2$) and triangularity ($n=3$) for the two considered approaches. We note that the results are close to each other, with somewhat smaller tails for the case of the wounded quarks (solid lines) for $n=2$, which moves the model a bit further from the data compared the the case of the wounded nucleons (dashed lines).

A long-standing problem for the Glauber-based simulations was the results for the ^{238}U+^{238}U collisions, measured at RHIC at $\sqrt{s_{NN}} = 200$ GeV [69]. It had been expected that owing to the intrinsic prolate deformation of the ^{238}U nucleus, the results of the most central collisions for the ellipticity should exhibit a knee structure [70]. It was later argued [30] that this structure may be washed out with large fluctuations

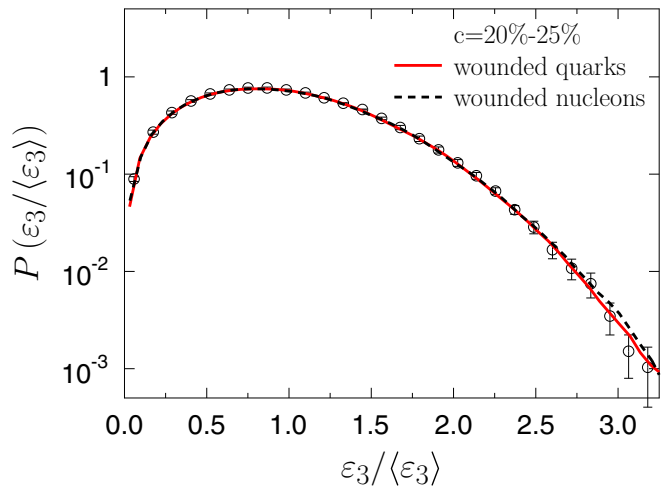

FIG. 6. Same as in Fig. 5 but for the triangularity ε_3.

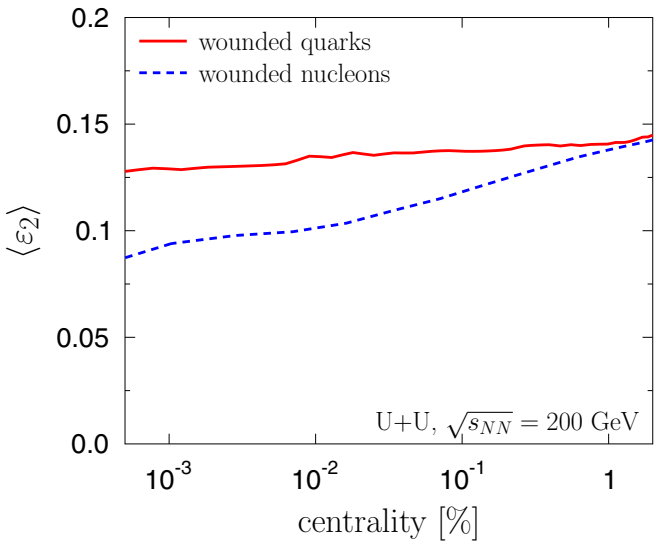

FIG. 7. Ellipticity ε_2 for the ^{238}U + ^{238}U collisions at $\sqrt{s_{NN}} = 200$ GeV for the wounded-quark (solid line) and wounded-nucleon (dashed line) models, plotted for centralities less than 1%.

of the overlaid distribution. Also, as shown recently, in a Glauber approach with *shadowing* [71] the model predictions compare well to the data. Here we compare the predictions of the wounded-quark and wounded-nucleon models. It is evident from Fig. 7 that at hypercentral collision the wounded-nucleon model leads to falloff of ellipticity with decreasing centrality c, whereas wounded quarks give a flattening, i.e., no knee behavior, in qualitative accordance to the data and the wounded-quark model studies reported in Ref. [69].

C. Size fluctuations

In Ref. [50] it was proposed that transverse size fluctuations of the initial state lead to transverse momentum fluctuations. The mechanism is based on the simple fact that more compressed matter, as may happen from statistical fluctuations in the initial state, leads to more rapid radial hydrodynamic expansion, which then provides more momentum to hadrons. The mechanism was later tested with $3 + 1$-dimensional viscous event-by-event hydrodynamics [72], with a somewhat surprising result that the effect leads to even larger (by about 30%) fluctuations than needed to explain the experimental data [73,74], in particular for most central collisions. The basic formula for the mechanism of Ref. [50] is that the event-by-event scaled standard deviation of the average transverse momentum is proportional to the corresponding quantity for the transverse size, $\langle r \rangle$, of the initial state,

$$\frac{\Delta\langle r\rangle}{\langle\langle r\rangle\rangle} = \beta \frac{\Delta\langle p_T\rangle}{\langle\langle p_T\rangle\rangle}, \tag{11}$$

where $\langle\langle\cdot\rangle\rangle$ denotes the event-by-event average of the quantity averaged in each event, Δ denotes the standard deviation, and the measure of the transverse size is

$$\langle r\rangle^2 = \frac{\int dxdys(x,y)(x^2+y^2)}{\int dxdys(x,y)}. \tag{12}$$

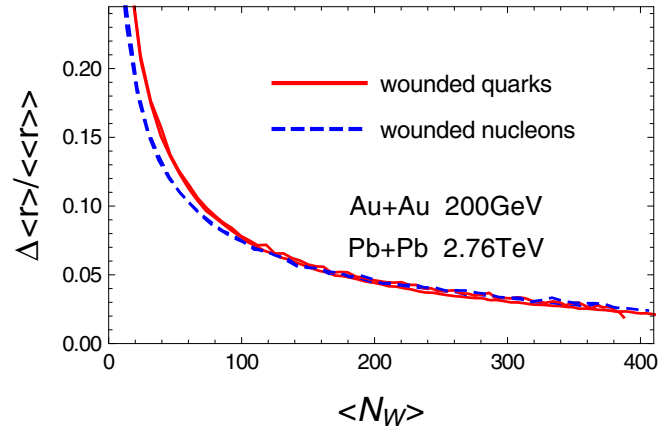

FIG. 8. Scaled size fluctuations of the initial fireball, plotted as a function of centrality evaluated in the wounded-quark and -nucleon models with an overlaid Γ distribution. The results for Au + Au at $\sqrt{s_{NN}} = 200$ GeV and Pb + Pb at $\sqrt{s_{NN}} = 2.76$ TeV overlap.

The function $s(x,y)$ is the entropy density in the transverse coordinates (x,y). The constant $\beta \sim 0.3$ depends on the hydrodynamic response, but not on the centrality of the collision, which allows for predictions. We introduce the variable

$$\langle r\rangle = \sqrt{\langle r\rangle^2}, \tag{13}$$

which is analyzed event by event; in particular, $\langle\langle r\rangle\rangle$ is the event-by-event average of the size of Eq. (13).

The results for the event-by-event scaled standard deviation of the size are presented in Fig. 8. We compare the wounded-nucleon (1) and the wounded-quark (2) models with an overlaid Γ distribution. We note that at low centralities the size fluctuations in both models are very close for the central collisions, whereas for peripheral collisions the size fluctuations are larger in the wounded-quark model. The results for the two sample reactions, Au + Au at $\sqrt{s_{NN}} = 200$ GeV and Pb + Pb at $\sqrt{s_{NN}} = 2.76$ TeV, are virtually indistinguishable, as the corresponding curves lie on top of each other.

IV. $p + A$ COLLISIONS

Ultrarelativistic $p + A$ collisions are an important testing ground for theoretical approaches, owing to the expected onset of collectivity [39,75–77]. It is thus important to address this issue with the model based on wounded quarks, as we search a uniform description of particle production. In this section we present the results for hadron multiplicity, the fireball size, and eccentricities.

A. Multiplicity distribution

To reproduce the experimental hadron multiplicity distribution in $p + A$ collisions, in particular the tail at very high multiplicities, one needs to overlay an additional distribution over the Glauber sources, as explained in Sec. II B. The physical meaning of this procedure is that sources deposit entropy at a varying strength. The mechanism was already proposed in the original wounded-nucleon model [1]. Experimental data are well reproduced with an overlaid negative

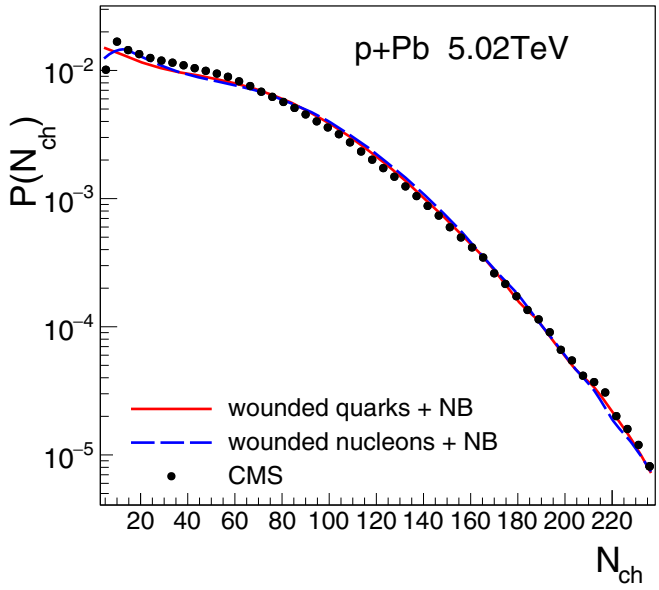

FIG. 9. Multiplicity of charged hadrons in $p+\mathrm{Pb}$ collisions from the wounded-quark and wounded-nucleon models, compared to the preliminary CMS data [78]. Appropriate negative binomial distribution is overlaid over the distribution of sources (see text).

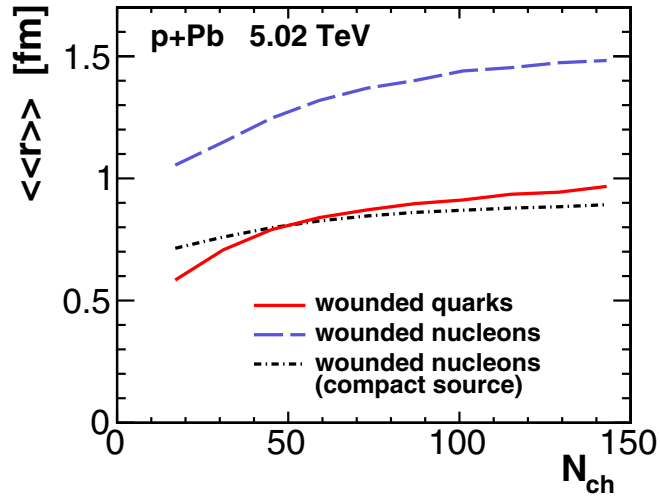

FIG. 10. Initial size of the fireball in $p+\mathrm{Pb}$ collisions at $\sqrt{s_{NN}} = 5.02$ TeV evaluated from Eq. (13) and plotted against the multiplicity of produced charged hadrons. The solid line corresponds to the wounded-quark model with the smearing parameter $\sigma = 0.2$ fm and is compared to wounded nucleons with $\sigma = 0.4$ fm in the standard form (dashed line) and the *compact source* version (dot-dashed line).

binomial distribution (Sec. II B). In Fig. 9 we compare the wounded-nucleon and the wounded-quark model predictions, compared to the CMS data [78]. The high-multiplicity tail is properly reproduced when the κ parameter of the negative binomial distribution is about 0.5. In Fig. 9 we use $\kappa = 0.54$ for the wounded-quark model, whereas $\kappa = 0.9$ for the wounded-nucleon model [$\alpha = 0$ in Eq. (1)]. Here we follow the convention that the parameters of the negative binomial distribution correspond to overlaying over the nucleons and not the nucleon pairs, as implied by Eq. (1). The parameter $\bar{n}$ is adjusted such that mean experimental multiplicities are reproduced at a given experimental acceptance and efficiency, namely $\bar{n} = 3.9$ for the wounded quark and $\bar{n} = 6.2$ for wounded nucleon.

We note a fair description of the tail of the distributions in Fig. 9, whereas, admittedly, there are departures at low values of N_{ch}.

In Fig. 9 the coordinate N_{ch} corresponds to the number of tracks in the CMS detector. Unfortunately, no hadron multiplicity data corrected for acceptance and efficiency are available, such that, at present, we cannot overlay the $p+\mathrm{Pb}$ point on other results in Fig. 1.

B. Fireball in $p+\mathrm{Pb}$

The size and the shape of the fireball are important characteristics of the initial state. The size of the fireball determines the transverse push and interferometry correlations [79], whereas the eccentricities generate harmonic flow coefficients in the collective expansion. In the hydrodynamic model the best description of the data is obtained when the entropy is deposited between the two colliding nucleons, in the so-called *compact source* scenario [39,80], where the entropy is deposited in the middle between the two colliding nucleons. The prescription corresponds to Eq. (1), with $\alpha = 1$. The effective number of sources is $N_{\mathrm{W}} - 1$ in this case, and the parameters of the overlaid binomial distribution fitted to the experiment as in Fig. 9 are $\bar{n} = 6.6$ and $\kappa = 1.0$.

In Fig. 10 we show the size measure of Eq. (13) plotted as a function of the number of produced charged hadrons. We note that the results from the wounded-quark model are closer to the *compact source* variant of the wounded nucleon model than to its standard version. Therefore, the wounded-quark model gives a microscopic motivation for the prescription used in the *compact source* scenario [39].

In Fig. 11 we present the ellipticity and the triangularity in the wounded-quark model. The deformation of the initial fireball is similar as in the standard wounded-nucleon model [39]. We expect that the shape and size of the fireball obtained in the wounded-quark model is a good initial condition for the hydrodynamic description of measurements made in $p+\mathrm{Pb}$ collisions.

V. $p+p$ COLLISIONS

With subnucleonic degrees of freedom we have an opportunity to analyze the $p+p$ collisions. The proton-proton inelastic collision profile in the wounded-quark model is described using quark-quark collisions (Sec. II A and the Appendix). The total inelastic cross section at each energy is reproduced with an energy-dependent quark-quark cross section.

A. Multiplicity distributions

The mean number of wounded quarks in $p+p$ collisions increases mildly with the energy, as we find $Q_{\mathrm{W}} = 2.6$, 2.75, and 2.81 at $\sqrt{s} = 200$ GeV, 2.76 TeV, and 7 TeV, respectively. The multiplicity of charged hadrons comes from a convolution

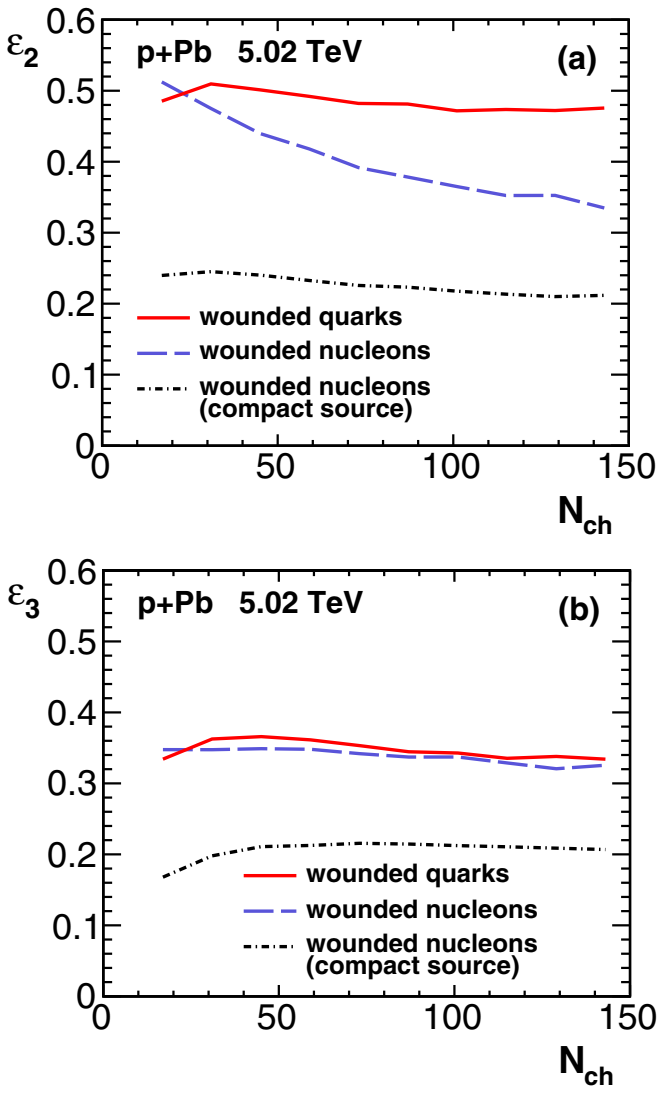

FIG. 11. Ellipticity (a) and triangularity (b) of the initial fireball in $p + \mathrm{Pb}$ collisions at $\sqrt{s_{NN}} = 5.02$ TeV from the wounded-quark model with smearing parameter $\sigma = 0.2$ fm, plotted as functions of the multiplicity of produced charged hadrons.

of the multiplicity distributions of particles produced from each wounded quark and the distribution of the number of wounded quarks (Sec. II B).

In Fig. 12 we show the multiplicity distribution of charged hadrons (for the acceptance window $|\eta| < 1$) in inelastic $p + p$ collisions at two energies: 2.76 and 7 TeV. The experimental results are represented by a numerical parametrization using a sum of two negative binomial distributions [55]. These curves for the multiplicity distributions are reproduced in the wounded-quark model by adjusting the parameters of the negative binomial distribution convoluted with the wounded-quark distribution. We find $\bar{n} = 3.3$ and $\kappa = 0.52$ at 7 TeV and $\bar{n} = 2.8$ and $\kappa = 0.55$ at 2.76 TeV (dotted lines in Fig. 12). The agreement of our model with the ALICE phenomenological fit, while not perfect, holds approximately over 12 orders of magnitude.

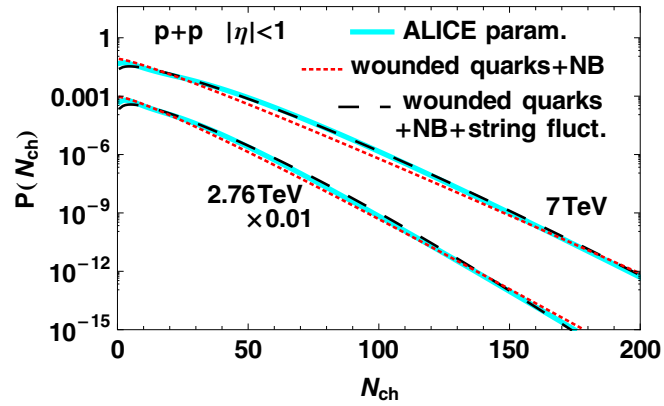

FIG. 12. Charged-particle multiplicity distribution for $|\eta| < 1$. Solid lines denote a parametrization of experimental data from the ALICE Collaboration [55] for $\sqrt{s} = 7$ TeV (upper curves) and for $\sqrt{s} = 2.76$ TeV (lower curves, multiplied by 0.01). The multiplicity distribution from the wounded-quark model convoluted with a negative binomial distribution is denoted with dotted lines, whereas dashed lines represent the calculation where both string fluctuations in rapidity and a negative binomial distribution are convoluted for each wounded quark.

The scenario discussed above assumes that all the wounded quarks contribute to particle production in the considered pseudorapidity interval. Alternative scenarios are possible, where each wounded quark contributes to particle production in a limited pseudorapidity interval. An example of such a case is the flux tube model, where strings decay into particles in a rapidity interval limited by the rapidity of the leading charges [81–83]. Without entering into details of a particular model of the random deposition of entropy in rapidity, we make a simple estimate using an extreme scenario. Namely, a wounded quark contributes (or not) with probability 1/2 to hadron production in the central rapidity interval. It is a scenario assuming largest possible fluctuations from a flux-tube mechanism. The goal of this exercise is to show that in both extreme scenarios, equal, smooth-in-rapidity contribution from each wounded quark and strongly fluctuating contribution from each quark, the observed hadron multiplicity distribution can be reproduced. In the model with fluctuating contribution from each wounded quark, the parameters of the negative binomial distribution are $\bar{n} = 7.9$ and $\kappa = 1.7$ at 7 TeV, and $\bar{n} = 7.4$ and $\kappa = 2.2$ at 2.76 TeV (dashed lines in Fig. 12). These estimates show that in the wounded-quark model there is a possibility to accommodate for a mechanism involving additional fluctuations in the energy deposition in a fixed rapidity interval, with a proper adjustment of the parameters of the convoluted negative binomial distribution.

B. Fireball in $p + p$

In an inelastic $p + p$ collisions two or more wounded quarks take part in the collision. The distribution of the wounded quarks in the transverse plane generates transverse shape deformations of the initial fireball. In such a small system it is essential to check the sensitivity to the range of the deposition of entropy from each quark. We take a Gaussian

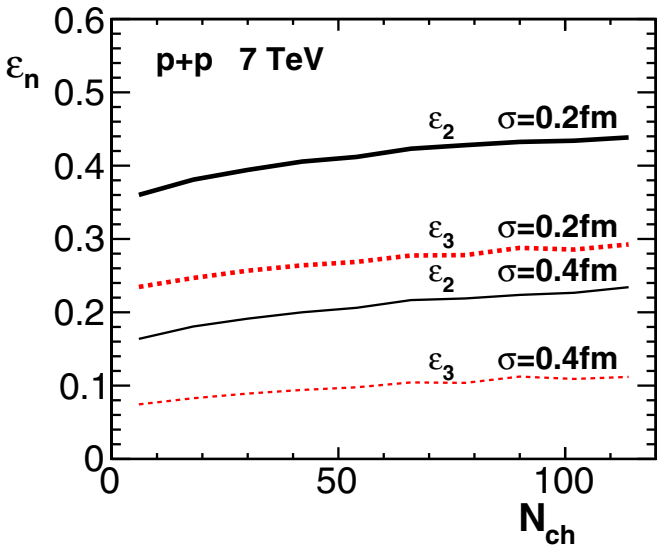

FIG. 13. Ellipticity ε_2 (solid lines) and triangularity ε_3 (dotted lines) of the fireball in $p+p$ collisions at $\sqrt{s} = 7$ TeV with the smoothing width $\sigma = 0.2$ fm (thick lines) and 0.4 fm (thin lines), as a function of the mean charged multiplicity for $|\eta| < 2.4$.

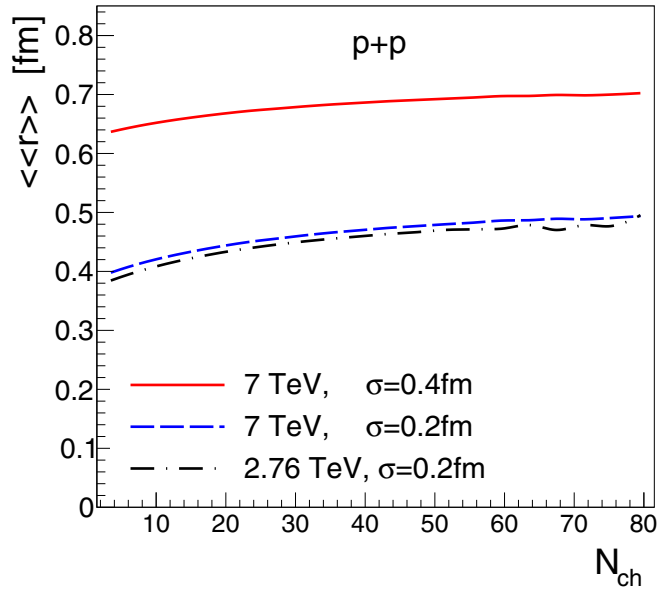

FIG. 14. Initial size of the fireball in $p+p$ collisions at the LHC energies evaluated with different Gaussian smearing parameters and plotted against the multiplicity of produced charged hadrons.

profile (9) of width of 0.2 or 0.4 fm. The distribution in the transverse plane takes into account the fluctuations in the entropy deposition from each wounded quark, with an overlaid Γ distribution with parameters adjusted to the multiplicity distribution as explained above. The total entropy in the fireball is rescaled to the mean multiplicity for $|\eta| < 2.4$. The eccentricities show a very weak dependence on multiplicity (Fig. 13). We note that the triangularity is much smaller than the ellipticity. In a scenario with a collective expansion in $p+p$ collisions, this would give v_3 much smaller than v_2. The smoothing parameter of the Gaussian in the initial fireball has a decisive role in determining the magnitude of the eccentricity.

In Fig. 14 we display the average size of the system formed in $p+p$ collisions at two LHC energies and for two values of the Gaussian smearing parameters. This observable reflects the size of the proton, the quark-quark inelasticity profile, and the Gaussian smearing parameter. We note that the size, especially for the case of $\sigma = 0.4$ fm, is not much smaller than in the $p+\mathrm{Pb}$ system shown in Fig. 10. This opens the opportunity of using the fireball from the wounded-quark model in hydrodynamic calculations for $p+p$ collisions [84,85].

VI. MORE PARTONS

The number of effective subnucleonic degrees of freedom in the nucleon could be different from three, where quark constituents are assumed. For instance, at the ISR energies the proton-proton scattering amplitude can be very well described using a quark-diquark model of the nucleon [86,87]. In the preceding sections we have assumed that the proton is composed of three quarks, as used in many other recent studies [14,18,21,22]. If protons are composed of numerous N_p partons, proton-proton collisions can be described in the Glauber optical model [88]. In the optical limit, the parameter defining the inelastic collisions is $N_p^2\sigma_{pp}$, where σ_{pp} is the parton-parton cross section. Similarly, in the Monte Carlo Glauber model, when the number of partons in the proton increases, the parton-parton cross section decreases. A model with different numbers of partons in the proton was recently studied by Loizides [23], with a black-disk prescription for the parton-parton scattering. The cross section σ_{pp} can then be adjusted to reproduce σ_{NN} for each N_p. It was found that with a large number of partons in a nucleon the increase of the number of wounded partons when going from peripheral to central events is stronger.

In our study we adjust the distribution profile of partons in the nucleon, as well as σ_{pp} and the parameters of the parton-parton inelastic scattering profile to reproduce the inelasticity profile in $p+p$ scattering, in the same way as for $N_p = 3$, as presented in the Appendix. We find $\sigma_{pp} = 22.96$, 11.93, 7.32, and 4.96 mb for $N_p = 2$, 3, 4, and 5, respectively. The relation $\sigma_{pp} \propto 1/N_p^2$ holds only approximately for the considered small number of partons in the nucleon.

The number of produced hadrons in $A+A$ collisions is taken as proportional to the number of wounded partons. The reduction of the cross section with the number of partons in the nucleon means that the number of wounded partons approaches the binary scaling in the Glauber model. It means that with decreasing parton-parton cross section the number of produced hadrons as a function of centrality interpolates between the wounded-nucleon scaling and the binary scaling. This dependence can be used to estimate the effective number of partons involved in inelastic nucleon-nucleon collisions. The charged-particle density in $\mathrm{Pb}+\mathrm{Pb}$ collisions divided by the number of partons is shown in Fig. 15. We notice that the number that best describes the scaling of the particle multiplicity is 3 or slightly above, where the curve is flat as a function of centrality. This argument gives support to results

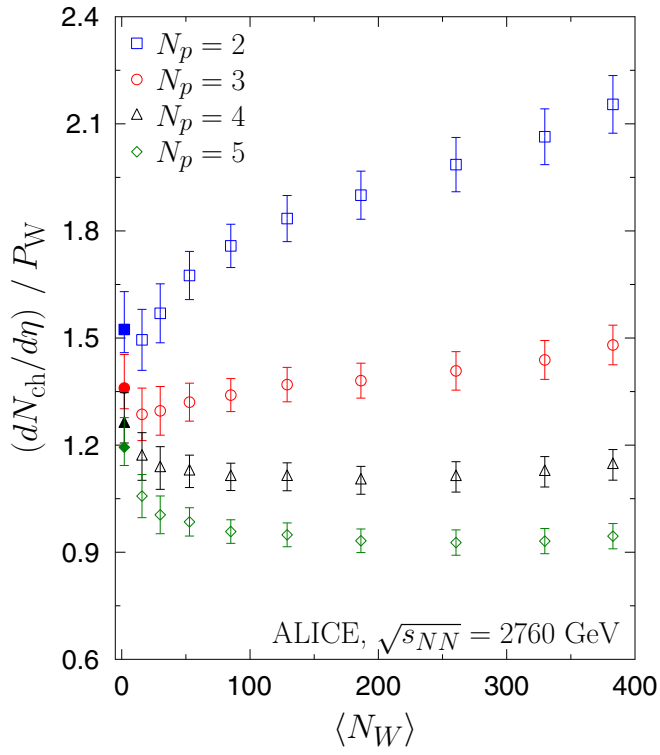

FIG. 15. The average multiplicity per unit of pseudorapidity, $dN_{\rm ch}/d\eta$, divided by the number of wounded partons $P_{\rm W}$ for the Pb + Pb collisions at $\sqrt{s_{NN}} = 2.76$ TeV (open symbols), evaluated with different numbers of constituent quarks in the nucleon, $N_{\rm W}$. The solid symbols at $\langle N_{\rm W} \rangle = 2$ correspond to $p + p$ collisions.

for collisions at the LHC energies presented in the preceding sections, where $N_p = 3$ was used.

VII. CONCLUSIONS

We have explored in detail the Glauber Monte Carlo implementation of the wounded-quark model, applied to particle production and for calculating the characteristics of the initial state in ultrarelativistic heavy-ion collisions. We have applied the model to $p + p$, $p + A$, $d + A$, He + A, Cu + Au, Au + Au, U + U, and Pb + Pb collisions at RHIC and the LHC energies, confirming an approximate linear scaling of the charged hadron density at midrapidity with the number of wounded quarks.

To constrain the parameters of the effective subnucleonic degrees of freedom in the nucleon, we reproduce the proton-proton inelasticity profile in the impact parameter by adjusting the distribution of quarks in the nucleon and the quark-quark inelasticity profile. We find that the effective size of the proton increases weakly with the collision energy, whereas the growth of the quark-quark cross section is substantial and is responsible for the increase of the inelastic nucleon-nucleon cross section. The multiplicity distributions in $p + p$ and p + Pb collisions are used to constrain the overlaid entropy fluctuations, here taken as an additional Γ distribution superposed over the distribution of the initial Glauber sources.

Our conclusions are as follows:

(1) The production of particles at midrapidity follows the wounded-quark scaling, with the quantity $dN_{\rm ch}/d\eta/Q_{\rm W}$ displaying approximately a flat behavior with centrality (cf. Fig. 1). This confirms the earlier reports [14,15,18,21] of the wounded-quark scaling, but with phenomenologically motivated parameters of the quark-quark interaction. At the LHC collision energy of $\sqrt{s_{NN}} = 2.76$ TeV the production per wounded quark in Pb + Pb collisions is compatible with the analogous quantity in $p + p$ collisions, which is an essential feature for the consistency of the approach, displaying the universality of the particle production based on superposition of individual collisions.

(2) At lower collision energies, such as $\sqrt{s_{NN}} = 200$ GeV, the universality is far from perfect and the obtained scaling is approximate, exhibiting some dependence on the reaction. Moreover, we note in Fig. 1 that the corresponding $p + p$ point is higher by about 30% from the band of other reactions. This indicates that at lower energies there are corrections to the independent production from the wounded quarks. Also, this may suggest a smaller number of effective subnucleonic degrees of freedom than three at these energies.

(3) Average eccentricities and their event-by-event fluctuations show a similar dependence on centrality in the wounded-quark model and in the wounded-nucleon model amended with binary collisions of Eq. (1). The average eccentricities are somewhat larger in the wounded-quark model compared to the wounded-nucleon case, reflecting the presence of additional fluctuations at subnucleonic scales.

(4) For collisions of the deformed U + U nuclei at RHIC ($\sqrt{s_{NN}} = 200$ GeV), we find that the average ellipticity in the wounded-quark model flattens at very central collisions, as opposed to the wounded-nucleon case. This is qualitatively in agreement with the absence of the knee structure in v_2 in experimental data.

(5) Event-by-event fluctuations of the initial size, responsible for the transverse-momentum fluctuations, are very similar in the wounded-quark model and in the wounded-nucleon model amended with binary collisions, with wounded quarks yielding somewhat larger values for peripheral collisions.

(6) The analysis of the distribution of particles at high multiplicity in p + Pb and $p + p$ collisions at the LHC energies shows that the needed overlaid distribution, taken in the negative binomial form, receives the same parameters. This is needed for the consistency of the approach.

(7) For p + Pb collisions, we find that the size and the eccentricity of the fireball is similar as in the *compact source* implementation of the wounded-nucleon model that best describes the data after the hydrodynamic evolution. In that way, we reduce the uncertainty in the initial conditions in small systems and obtain a more microscopic motivation for mechanism of the entropy deposition in the initial stage.

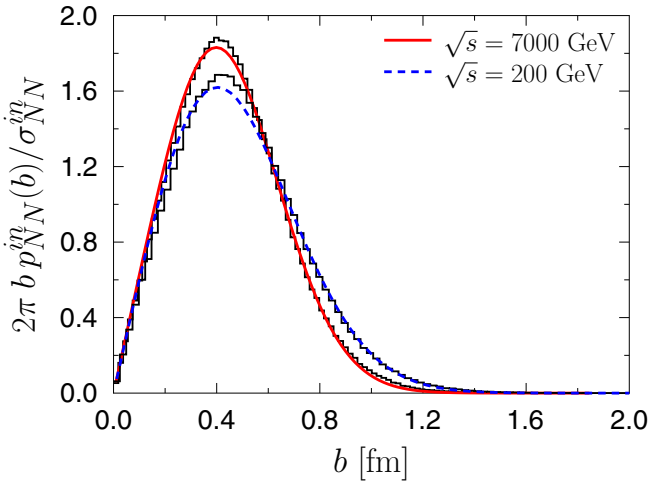

FIG. 16. Inelasticity profiles $2\pi b p^{\rm in}_{NN}$ obtained from folding three quarks (thick dashed line for $\sqrt{s} = 200$ GeV and thick solid line for $\sqrt{s} = 7$ TeV), compared to the parametrization of Ref. [32] (thin solid lines), plotted as functions of the impact parameter b.

(8) For $p + p$ collisions we generate initial fireballs which later may be used in hydrodynamic studies. It is expected that the resulting triangular flow should be much smaller from the elliptic flow.
(9) We have also tested the hypothesis that the effective number of partons in the nucleon is smaller or larger than three. However, particle production data at the LHC are fairly well described using three partons, identified with constituent (wounded) quarks.

ACKNOWLEDGMENTS

We thank Andrzej Białas, Adam Bzdak, Constantin Loizides, and Jurgen Schukraft for useful discussions. Research supported by the Polish Ministry of Science and Higher Education, (MNiSW), by National Science Centre, Poland Grants No. DEC-2015/17/B/ST2/00101 and No. DEC-2012/06/A/ST2/00390.

APPENDIX: QUARK-QUARK WOUNDING PROFILE

In this Appendix we present in detail our procedure of fixing the inelasticity profile of the quark-quark collisions, based on the experimental NN scattering data. The inelasticity profile in NN collisions is defined via the NN scattering amplitude

$$p^{\rm in}_{NN}(b) = 4p[{\rm Im}h(b) - p|h(b)|^2], \qquad \text{(A1)}$$

where b is the impact parameter, p is the CM momentum of the nucleon, and in the eikonal approximation $bp = l + 1/2 + \mathcal{O}(s^{-1})$ the scattering amplitude is $h(b) = f_l(p) + \mathcal{O}(s^{-1})$. Following the lines of Ref. [89], we take a working parametrization for $h(b)$ from Ref. [31], whose functional form is based on the Barger-Phillips model [32].

When the nucleon is composed of three constituent quarks, its inelasticity is a folding of the inelasticity of the quark and the distribution of quarks in the nucleon. Here we proceed in an approximate way, using the expressions (3,4). The shape of the resulting NN inelasticity profile is determined be dimensionless ratio $\sigma_{\rm qq}/r_0^2$, whereas the normalization, i.e., the NN inelastic cross section $\sigma^{\rm in}_{NN} = \int 2\pi b db\, p^{\rm in}_{NN}(b)$, is controlled with $\sigma_{\rm qq}$. A sample result of the fit for $\sqrt{s_{NN}}$ is shown in Fig. 16. Richer functional forms of Eqs. (3,4) would allow for an even better agreement, but for the present application the accuracy is by far sufficient.

In Table I we give the obtained values of model parameters for various collision energies. As the experimental $p^{\rm in}_{NN}(b)$ may be very well approximated with the Γ profile of Ref. [90],

$$p^{\rm in}_{NN}(b) = A\Gamma\left[1/\omega, \pi A b^2 \big/ \left(\omega\sigma^{\rm in}_{NN}\right)\right] / \Gamma(1/\omega), \qquad \text{(A2)}$$

with $\Gamma(a,x)$ denoting the incomplete Euler Γ function, we also list parameters A and ω in Table I, as well as the inelastic NN cross section $\sigma^{\rm in}_{NN}$.

We note that the size parameter r_0 in Table I corresponds to the rms radius of the nucleon (including the CM corrections as obtained from the Monte Carlo simulation) equal from 0.70 fm at $\sqrt{s_{NN}} = 17.3$ GeV to 0.84 fm at $\sqrt{s_{NN}} = 7$ TeV. This range is comparable to estimates for the size of the nucleon.

TABLE I. Parameters of the quark distribution in the nucleon of Eq. (3), r_0, quark-quark inelastic cross section of Eq. (4), $\sigma_{\rm qq}$, as well as parameters A and ω from Eq. (A2) for various NN collision energies. The last column lists the total inelastic nucleon-nucleon cross section $\sigma^{\rm in}_{NN}$.

$\sqrt{s_{NN}}$ (GeV)	r_0 (fm)	$\sigma_{\rm qq}$ (mb)	A	ω	$\sigma^{\rm in}_{NN}$ (mb)
17.3	0.25	5.1	0.94	0.83	31.5
62.4	0.27	5.8	0.92	0.79	35.6
130	0.27	6.5	0.97	0.80	38.8
200	0.27	7.0	0.97	0.76	41.3
2760	0.29	11.9	0.99	0.57	64.1
5020	0.30	13.6	1.0	0.53	70.9
7000	0.30	14.3	1.0	0.51	74.4

[1] A. Białas, W. Czyż, and W. Furmański, Acta Phys. Polon. **B8**, 585 (1977); A. Białas, K. Fiałkowski, W. Słomiński, and M. Zieliński, *ibid.* **B8**, 855 (1977); A. Białas and W. Czyż, *ibid.* **B10**, 831 (1979).
[2] V. V. Anisovich, Yu. M. Shabelski, and V. M. Shekhter, Nucl. Phys. B **133**, 477 (1978).
[3] A. Białas, M. Błeszyński, and W. Czyż, Nucl. Phys. B **111**, 461 (1976).
[4] R. J. Glauber, in *Lectures in Theoretical Physics*, edited by W. E. Brittin and L. G. Dunham (Interscience, New York, 1959), Vol. 1, p. 315.
[5] W. Czyż and L. C. Maximon, Ann. Phys. **52**, 59 (1969).

[6] A. Białas, J. Phys. G **35**, 044053 (2008).
[7] B. B. Back *et al.* (PHOBOS Collaboration), Phys. Rev. C **65**, 031901(R) (2002).
[8] D. Kharzeev and M. Nardi, Phys. Lett. B **507**, 121 (2001).
[9] B. Schenke, P. Tribedy, and R. Venugopalan, Phys. Rev. Lett. **108**, 252301 (2012).
[10] A. Adil, H.-J. Drescher, A. Dumitru, A. Hayashigaki, and Y. Nara, Phys. Rev. C **74**, 044905 (2006).
[11] J. S. Moreland, J. E. Bernhard, and S. A. Bass, Phys. Rev. C **92**, 011901 (2015).
[12] S. Eremin and S. Voloshin, Phys. Rev. C **67**, 064905 (2003).
[13] P. K. Netrakanti and B. Mohanty, Phys. Rev. C **70**, 027901 (2004).
[14] S. S. Adler *et al.* (PHENIX Collaboration), Phys. Rev. C **89**, 044905 (2014).
[15] A. Adare *et al.* (PHENIX Collaboration), Phys. Rev. C **93**, 024901 (2016).
[16] B. Alver, M. Baker, C. Loizides, and P. Steinberg, arXiv:0805.4411 [nucl-ex].
[17] C. Loizides, J. Nagle, and P. Steinberg, SoftwareX **1-2**, 13 (2015).
[18] R. A. Lacey, P. Liu, N. Magdy, M. Csand, B. Schweid, N. N. Ajitanand, J. Alexander, and R. Pak, arXiv:1601.06001 [nucl-ex].
[19] G. Agakishiev *et al.* (STAR Collaboration), Phys. Rev. C **86**, 014904 (2012).
[20] A. Białas and A. Bzdak, Phys. Lett. B **649**, 263 (2007); Phys. Rev. C **77**, 034908 (2008).
[21] L. Zheng and Z. Yin, Eur. Phys. J. A **52**, 45 (2016).
[22] J. T. Mitchell, D. V. Perepelitsa, M. J. Tannenbaum, and P. W. Stankus, Phys. Rev. C **93**, 054910 (2016).
[23] C. Loizides, arXiv:1603.07375 [nucl-ex].
[24] W. Broniowski, M. Rybczyński, and P. Bożek, Comput. Phys. Commun. **180**, 69 (2009).
[25] Q. Y. Shou, Y. G. Ma, P. Sorensen, A. H. Tang, F. Videbk, and H. Wang, Phys. Lett. B **749**, 215 (2015).
[26] M. Alvioli, H.-J. Drescher, and M. Strikman, Phys. Lett. B **680**, 225 (2009).
[27] U. W. Heinz and A. Kuhlman, Phys. Rev. Lett. **94**, 132301 (2005).
[28] P. Filip, Phys. Atom. Nucl. **71**, 1609 (2008).
[29] P. Filip, R. Lednicky, H. Masui, and N. Xu, Phys. Rev. C **80**, 054903 (2009).
[30] M. Rybczyński, W. Broniowski, and G. Stefanek, Phys. Rev. C **87**, 044908 (2013).
[31] D. A. Fagundes, G. Pancheri, A. Grau, S. Pacetti, and Y. N. Srivastava, Phys. Rev. D **88**, 094019 (2013).
[32] R. J. N. Phillips and V. D. Barger, Phys. Lett. B **46**, 412 (1973).
[33] U. Heinz and J. S. Moreland, Phys. Rev. C **84**, 054905 (2011).
[34] A. Giovannini and L. Van Hove, Z. Phys. C **30**, 391 (1986).
[35] J. I. Kapusta, B. Muller, and M. Stephanov, Phys. Rev. C **85**, 054906 (2012).
[36] S. Gavin, L. McLerran, and G. Moschelli, Phys. Rev. C **79**, 051902 (2009).
[37] L. Yan and H. Grönqvist, J. High Energy Phys. 03 (2016) 121.
[38] M. Rybczyński, G. Stefanek, W. Broniowski, and P. Bożek, Comput. Phys. Commun. **185**, 1759 (2014).
[39] P. Bożek and W. Broniowski, Phys. Rev. C **88**, 014903 (2013).
[40] I. Kozlov, M. Luzum, G. Denicol, S. Jeon, and C. Gale, arXiv:1405.3976 [nucl-th].
[41] G. Baym, B. L. Friman, J. P. Blaizot, M. Soyeur, and W. Czyz, Nucl. Phys. A **407**, 541 (1983).
[42] J. P. Blaizot and J.-Y. Ollitrault, Nucl. Phys. A **458**, 745 (1986).
[43] B. Muller and A. Schafer, Int. J. Mod. Phys. E **20**, 2235 (2011).
[44] H. Song and U. W. Heinz, Phys. Rev. C **78**, 024902 (2008).
[45] P. Bożek, Phys. Rev. C **81**, 034909 (2010).
[46] R. J. Fries, B. Muller, and A. Schafer, Phys. Rev. C **78**, 034913 (2008).
[47] H. Niemi, G. S. Denicol, H. Holopainen, and P. Huovinen, Phys. Rev. C **87**, 054901 (2013).
[48] A. Bzdak, P. Bożek, and L. McLerran, Nucl. Phys. A **927**, 15 (2014).
[49] P. Bożek, W. Broniowski, E. R. Arriola, and M. Rybczyński, Phys. Rev. C **90**, 064902 (2014).
[50] W. Broniowski, M. Chojnacki, and L. Obara, Phys. Rev. C **80**, 051902 (2009).
[51] W. Broniowski and W. Florkowski, Phys. Rev. C **65**, 024905 (2002).
[52] W. Broniowski and M. Rybczyński, Phys. Rev. C **81**, 064909 (2010).
[53] J. Carlson and R. Schiavilla, Rev. Mod. Phys. **70**, 743 (1998).
[54] G. J. Alner *et al.* (UA5 Collaboration), Z. Phys. C **33**, 1 (1986).
[55] J. Adam *et al.* (ALICE Collaboration), arXiv:1509.07541 [nucl-ex].
[56] K. Aamodt *et al.* (ALICE Collaboration), Phys. Rev. Lett. **106**, 032301 (2011).
[57] G. Aad *et al.* (ATLAS Collaboration), J. High Energy Phys. 11 (2013) 183.
[58] J.-Y. Ollitrault, Phys. Rev. D **46**, 229 (1992).
[59] B. Alver *et al.* (PHOBOS Collaboration), Phys. Rev. Lett. **98**, 242302 (2007).
[60] S. A. Voloshin, arXiv:nucl-th/0606022.
[61] Y. Hama, R. Peterson G.Andrade, F. Grassi, W.-L. Qian, T. Osada *et al.*, Phys. Atom. Nucl. **71**, 1558 (2008).
[62] B. Alver and G. Roland, Phys. Rev. C **81**, 054905 (2010).
[63] M. Luzum, J. Phys. G **38**, 124026 (2011).
[64] R. S. Bhalerao, J.-Y. Ollitrault, and S. Pal, Phys. Lett. B **742**, 94 (2015).
[65] W. Broniowski, P. Bożek, and M. Rybczyński, Phys. Rev. C **76**, 054905 (2007).
[66] J.-P. Blaizot, W. Broniowski, and J.-Y. Ollitrault, Phys. Rev. C **90**, 034906 (2014).
[67] M. Luzum and J.-Y. Ollitrault, Nucl. Phys. A **904-905**, 377c (2013); J.-B. Rose, J.-F. Paquet, G. S. Denicol, M. Luzum, B. Schenke, S. Jeon, and C. Gale, *ibid.* **931**, 926 (2014).
[68] S. Chatrchyan *et al.* (CMS Collaboration), J. High Energy Phys. 02 (2014) 088; G. Aad *et al.* (ATLAS Collaboration), Phys. Rev. C **86**, 014907 (2012).
[69] L. Adamczyk *et al.* (STAR Collaboration), Phys. Rev. Lett. **115**, 222301 (2015).
[70] S. A. Voloshin, Phys. Rev. Lett. **105**, 172301 (2010).
[71] S. Chatterjee, S. K. Singh, S. Ghosh, M. Hasanujjaman, J. Alam, and S. Sarkar, Phys. Lett. B **758**, 269 (2016).
[72] P. Bożek and W. Broniowski, Phys. Rev. C **85**, 044910 (2012).
[73] S. Adler *et al.* (PHENIX Collaboration), Phys. Rev. Lett. **93**, 092301 (2004).
[74] J. Adams *et al.* (STAR Collaboration), Phys. Rev. C **72**, 044902 (2005).
[75] P. Bożek, Phys. Rev. C **85**, 014911 (2012).
[76] P. Bożek and W. Broniowski, Phys. Lett. B **718**, 1557 (2013).

[77] P. Bożek, W. Broniowski, and G. Torrieri, Phys. Rev. Lett. **111**, 172303 (2013).
[78] S. Chatrchyan *et al.* (CMS Collaboration), CMSPublic Web (2012), http://twiki.cern.ch/twiki/bin/view/CMSPublic/PhysicsResultsHIN12015.
[79] P. Bożek and W. Broniowski, Phys. Lett. B **720**, 250 (2013); B. Schenke and R. Venugopalan, Phys. Rev. Lett. **113**, 102301 (2014).
[80] A. Bzdak, B. Schenke, P. Tribedy, and R. Venugopalan, Phys. Rev. C **87**, 064906 (2013).
[81] B. Andersson, G. Gustafson, G. Ingelman, and T. Sjostrand, Phys. Rept. **97**, 31 (1983).
[82] P. Bożek and W. Broniowski, Phys. Lett. B **752**, 206 (2016).
[83] A. Monnai and B. Schenke, Phys. Lett. B **752**, 317 (2016).
[84] P. Bożek, Acta Phys. Pol. B **41**, 837 (2010).
[85] K. Werner, I. Karpenko, T. Pierog, M. Bleicher, and K. Mikhailov, Phys. Rev. C **83**, 044915 (2011).
[86] A. Białas and A. Bzdak, Acta Phys. Polon. B **38**, 159 (2007).
[87] T. Csörgő and F. Nemes, Int. J. Mod. Phys. A **29**, 1450019 (2014).
[88] D. d'Enterria *et al.*, Eur. Phys. J. C **66**, 173 (2010).
[89] E. Ruiz Arriola and W. Broniowski, Few Body Syst. **57**, 485 (2016).
[90] M. Rybczyński and Z. Włodarczyk, J. Phys. G **41**, 015106 (2013).